Contrib. Mineral. Petrol. 64, 167–195 (1977)

Contributions to Mineralogy and Petrology

Magma Fractionation Systems Beneath the Mid-Atlantic Ridge at 36–37° N

M.F.J. Flower[1], P.T. Robinson[2], H.-U. Schmincke[1], and W. Ohnmacht[1]

[1] Institut für Mineralogie der Ruhr-Universität, D-4630 Bochum, Federal Republic of Germany
[2] Department of Earth Sciences, University of California, Riverside, California, U.S.A.

Abstract. Variation of major and trace elements in drilled basalts from the Mid-Atlantic Ridge (DSDP Leg 37) reflects distinct cycles of low pressure fractionation operating independently within a complex network of magma storage reservoirs beneath the crustal spreading axis. Low pressure phase relations are determined by parental magma composition, which varies from *An*-rich (An/Di > ca. 1.4) to *Di*-rich (*An/Di* < ca. 1.4). High *An/Di* magmas probably formed under slightly hydrous conditions in the mantle. They have low LIL element contents, low P/Y and high Mg/(Mg+Fe) ratios. Zr, P and Y abundance and inter-element ratios are highly diagnostic of primary magma type, and are used to quantify fractional crystallization models.

Low pressure fractionation hypotheses were tested by least-squares modelling of whole-rock and phenocryst chemistry, which indicated removal or addition of phenocryst assemblages: ol; pl; ol+pl; ol+pl+cpx; pl+cpx, (±sp). Accumulation of plagioclase or olivine is an important mechanism for generating highly porphyritic rocks. A rare 3-phase (ol+pl+cpx) cumulate resulted from cotectic fractionation of a low *An/Di* magma type. Olivine and plagioclase cumulates appear to be related to high *An/Di* magmas. Olivine accumulation has been monitored by comparison of olivine/bulk rock partitioning of Fe and Mg to experimental measurements of the equilibrium K_D value. A single extensive sub-axial magma chamber could not account for the observed chemical variation and would probably be dynamically unstable.

Introduction

Most models for generation, evolution and emplacement of abyssal tholeiite magma at accretionary plate margins (e.g. Aumento, 1967; Cann, 1970, 1974;

Moore et al., 1974; Ballard et al.,1975) are based on the following assumptions: a) a perturbed geothermal gradient resulting from diapiric uprise of mantle peridotite beneath spreading axes; b) a high degree of partial melting at relatively low pressures (7–10 Kbars) (Kushiro,1973); c) the existence of extensive (possibly continuous) and volumetrically large magma reservoirs beneath the spreading axis to explain the chemically evolved character of abyssal basalt magmas through fractional crystallization; d) the formation of a layered crust comprising accreted plutonic material beneatah dike-swarm zone and an uppermost eruptive layer.

The information providing the basis of such models is derived largely from studies of ophiolites, worldwide dredge samples, subaerially exposed zones of crustal accretion (e.g. Iceland) and from detailed surveying by submersibles of the Atlantic median rift (the 'FAMOUS' project), together with experimental studies of basalt systems and measurements of seismicity, heat flow and magnetism of the oceanic crust. With the inception of IPOD (International Phase of Ocean Drilling), and the prospect of systematic deep drilling of ocean crust, we are now able to begin testing present hypotheses of crustal generation and putting forward new and refined models.

In this paper we report interpretations of geochemical data from the first successful attempt at deep penetration of the ocean crust, on the Mid-Atlantic Ridge (MAR) at 36° N, during Leg 37 of the Deep Sea Drilling Project (DSDP). Our purpose is to show how lithologic and chemical variability of eruptive rocks in one small segment of ocean crust can be explained by cycles of fractional crystallization operating in discrete intervals of time and space upon a variable range of parental basaltic magmas. The identification of individual 'systems' of fractional crystallization and their relations to the observed crustal stratigraphy provides several specific constraints on physical processes of crustal construction in mid-ocean ridges.

Drilling of acoustic basement to depths >100 m was achieved at four sites (332–335 incl.) on a sea-floor spreading flow line WNW of the 'FAMOUS'[1] region, ranging in age from 3.5 to about 13.5 m.y. (Melson et al., 1974). Five holes were drilled (332A, 332B, 333A, 334 and 335) penetrating respectively, 333 m, 583 m, 312 m, 118 m and 108 m into basement. Most of the recovered material comprises basalt, interlayered in part with calcareous sediment and basaltic breccia. However, at Site 334 a gabbro-peridotite complex was encountered, beneath a 50 m-thick sequence of basalt. Breccia zones within the plutonic complex consist exclusively of gabbro and peridotite fragments and many have nannochalk matrices. The melange at Site 334 is believed to have been intruded as a solid body at the median rift prior to burial by later eruptions (Melson et al., 1974).

Chemical data for the drilled rocks, and preliminary interpretations, have been presented in Initial Reports of the Deep Sea Drilling project, Vol. 37, and at symposia on the 'nature of oceanic crust' at Brest (Nov. 1975) and La Jolla (Dec. 1975). [e.g. Flower et al., 1977; Gunn and Roobol, 1977; Bryan et al., 1977]. Detailed lithologic descriptions for each site, studies of physical properties and magnetics, and specialized geochemical and isotopic studies are also included in the Initial Report.

[1] FAMOUS = 'French-American Mid-Ocean Undersea Survey'

Methods and Data

Data used in this study comprise analyses of bulk rocks, glass cooling rinds and phenocryst and groundmass phases. Approximately 150 whole-rock analyses were made by X-ray fluorescence for all major elements except Na, and for selected trace elements (Ba, Cr, Ni, Cu, Rb, Sr, Y and Zr) using Philips PW 1212 (Imperial College) and Philips PW 1410 (Bochum) instruments. Glass analyses were made by electron microprobe by W.G. Melson at the Smithsonian Institution, and are used here (with permission) in the form of averages of compositional groupings made by T.L. Wright of the U.S. Geological Survey (personal comm.). Both colleagues are gratefully acknowledged.

About 500 analyses of mineral phases were made by electron microprobe at ETH, Zürich, and about 20 at Imperial College. All data are reported in the DSDP Leg 37 Initial Report (Flower et al., 1977) accompanied by analyses of interlaboratory comparison samples and estimates of accuracy and precision. In this paper we give 25 representative bulk-rock analyses (Table 2) and compositional ranges of mineral phases as related to chemical groupings of whole rock data. Averages of glass groups are given in Table 1.

In interpreting the chemical variability of Leg 37 basalts we have postulated fractional crystallization models involving observed phenocryst phases, utilizing chemical data for whole-rock, fresh glass and phenocryst compositions. We have largely confined our attention to data for Holes 332A and 332B because these holes represent the deepest penetration to date into oceanic basement and because the recovered rocks can be genetically related in space and time.

Lithology

The first stage of interpreting the drilled ocean crust sections was to establish the major lithologic units (defined by abundance and relative proportion of phenocrysts, groundmass texture, etc.). Lithologic 'sub-units' are recognized from minor lithologic changes such as breccia and sediment intercalations, exceptionally vesicular zones or zones of alteration. Because of low recovery (averages range from 8% in Hole 333A to 38% in Hole 335), many individual flows and cooling units could have been missed in coring. However, some material was recovered from each 9.5 m core and there is a reasonable degree of lithologic and chemical continuity between material recovered from successively cored intervals. Hence, we assume that no *major* lithologies are missing from the schematic divisions made on shipboard (Melson et al., 1974).

Eruptive units are mostly pillowed but occasionally comprise massive sequences. Intrusive units are very hard to confirm and, if present, are inferred from the chemical stratigraphy to have been approximately coeval with the erupted lavas. The lithologic diversity at Sites 332 and 333 is accompanied by chemical and magnetic intensity variations over relatively short vertical intervals. Inter-hole stratigraphic correlation is likewise surprisingly poor.

In summary, cored basalts range from aphyric to very highly phyric. Phenocryst assemblages in highly phyric varieties are mostly *olivine ± Cr-spinel* (picrites), or *plagioclase ± (minor) olivine*, with the exceptional appearance of a 3-phase *olivine + plagioclase + clinopyroxene* assemblage at the base of Hole 332A. Moderately- to sparsely-phyric basalts have phenocryst assemblages of *olivine*, *olivine + plagioclase*, and *plagioclase + clinopyroxene ± olivine*. The lower part of Hole 332B shows complex interlayering of different lithologies. Hole 333A is probably similar but harder to evaluate due to poor recovery.

Low temperature alteration (halmyrolysis) is evidenced by the common presence of smectite and other secondary phases in Leg 37 basalts. A separate study of alteration phase chemistry has been made (Robinson et al., 1977) and suggests that with the exception of elements such as K, Ba, Rb, Sr, and in some cases Mg and Ca, bulk rock chemistry is generally indicative of erupted magma composition.

Chemical Variation of Leg 37 Basalts: Fractionation Hypotheses

An unexpectedly large range of chemical variation was found, although all Leg 37 basaltic compositions conform to olivine- or quartz-tholeiites of MORB (Mid-Ocean Ridge Basalt) type (Melson et al., 1976). The variation at Site 332 alone is probably as great as that observed for worldwide dredge sampling of MORB (e.g. MgO ranges 5–25 wt % for Hole 332B basalts).

Table 1. Average compositions of glass groups

	Site 332 Hole 332A					Site 332 Hole 332B
	332A-a	332A-b	332A-c	332A-d	332A-e	332B-a
SiO_2	51.28	51.91	51.10	51.67	50.99	51.52
TiO_2	1.03	1.19	1.25	1.13	1.23	1.16
Al_2O_3	14.82	14.58	14.81	14.66	14.42	14.87
FeO[a]	9.79	10.95	10.61	10.48	11.25	9.95
MnO[b]	0.20	0.20	0.20	0.20	0.20	0.20
MgO	7.62	6.70	7.46	7.47	7.09	7.77
CaO	12.49	11.41	11.91	11.97	11.59	12.40
Na_2O	2.07	2.30	2.10	2.12	2.20	2.02
K_2O	0.16	0.19	0.22	0.17	0.20	0.19
P_2O_5	0.10	0.11	0.13	0.11	0.10	0.11
Total	99.56	99.54	99.79	99.97	99.27	100.19
mg'[c]	0.616	0.554	0.589	0.592	0.560	0.616
No. of analyses	2	2	4	1	1	3
Core nos.	15 cc to 18 cc	22–1 to 25–1	26–1 to 26–2	40–1	40–2	8–1
Equiv. rock group	332A-2	332A-2	332A-3	?	?	332B-2

In this study we have extended the preliminary ship-board interpretations and attempted to define chemical groups more clearly, within which variation of chemistry and lithology can be explained by differential movement of phenocrysts in a single parent magma during its temporary storage in a sub-rift magma chamber. Assuming phenocrysts to be formed at shallow levels, such groups may be taken to represent 'low pressure fractionation systems' with discrete temporal and spatial identities, and whose *inter*relationships involve factors other than low pressure fractionation. Postulated chemical groupings were tested for consistency with these criteria by means of petrologic mixing calculations using the Mineral Distribution Program (MDP) of Wright and Doherty (1970).

It was not possible to achieve a rigorous statistical grouping of whole-rock analyses, partly due to discrepancies introduced by alteration effects, but mostly as a result of extensive linear variation contributed by phenocryst accumulation. Data for fresh glasses (W.G. Melson, pers. comm.) were divided by means of a chemical sorting program (T.L. Wright, pers. comm.) into 13 distinct chemically unique groupings, each with a stratigraphic identity, whose average compositions are given in Table 1.

Chemical groupings of whole-rock compositions were initially identified from orthogonal plots of whole-rock and mineral data in MgO-variation diagrams, and by graphical comparison with stratigraphically associated glass groups, (Flower et al., 1977). These groups also have a distinct stratigraphic identity. Representative analyses of magma groups thus postulated (numbered 332A-

Table 1 (continued)

					Sites 334 and 335		
	332B-b	332B-c	332B-d	332B-e	334	335-a	335-b
SiO_2	50.09	49.60	50.60	49.75	52.03	50.69	50.49
TiO_2	0.76	0.64	0.89	0.67	0.83	0.17	1.13
Al_2O_3	16.34	16.63	16.09	15.77	14.53	16.28	15.67
FeO[a]	9.32	9.09	10.03	8.74	9.86	9.59	9.39
MnO[b]	0.20	0.20	0.20	0.20	0.20	0.20	0.20
MgO	8.92	8.98	7.95	8.70	7.91	6.66	7.99
CaO	12.29	12.38	11.77	13.85	12.72	12.12	11.87
Na_2O	2.05	2.05	2.34	1.90	1.81	2.57	2.39
K_2O	0.11	0.07	0.07	0.07	0.08	0.17	0.17
P_2O_5	0.07	0.04	0.06	0.04	0.07	0.09	0.10
Total	100.15	99.68	100.00	99.69	100.04	99.54	99.40
mg′[c]	0.666	0.674	0.619	0.677	0.623	0.590	0.639
No. of analyses	2	6	8	3	4	1	24
Core nos.	19–1	20–2 to 25–2	22–2 to 25–2	36–1 to 36–4	16–5 to 19–2	5–2	5–2 to 14–3
Equiv. rock group	332B-3	332B-4	332B-5	332B-6	334-1	?	335

[a] Total Fe-oxide
[b] Assumed MnO
[c] $mg' = Mg/(Mg + Fe^{+2})$ calc. assuming $Fe_2O_3 = 1.5$ wt.%

1–6; 332B-1–7; or for brevity A-1–6; B-1–7; etc. with increasing depth of occurrence in respective profiles) are given in Table 2. On comparing their respective lithology and petrography we see that each group has a characteristic phenocryst (and microphenocryst) assemblage, which presumably accounts for distinctive intra-group variation trends. Work in progress (Ohnmacht et al., in prep.) shows that pyroxene, olivine and plagioclase solid solution trends are a sensitive indicator of the whole-rock intra-group fractionation. In Table 3, we give compositional ranges observed for the principal phenocryst phases, as related to host magma groups identified from whole-rock chemistry.

A schematic diagram of whole-rock oxide versus MgO variation is given in Figure 1, adapted from the data plots in Flower et al., 1977. The most diagnostic elements are clearly Ti, P, Al, Ca and Fe for any one value of MgO content. The fractionation trends may be provisionally interpreted as due to:

(a) olivine accumulation, (332B-3, -4, -6a);
(b) plagioclase accumulation; (332A-1, -4, 332B-1, -2, -6b);
(c) olivine + plagioclase removal; (332B-5);
(d) plagioclase + clinopyroxene + olivine removal; (332A-2, -3, 332B-2);
(e) olivine + plagioclase + clinopyroxene accumulation (?); (332A-5).

Table 2. Representative analyses of Leg 37 magma groups (normalized to a volatile-free basis)

Magma group:	332A-1	332A-2	332A-3	332A-4	332A-5	332A-6	332B-1	332B-2	332B-3
DSDP sample No. (core section cm interval)	7–1 (66–68)	23–1 (26–27)	26–1 (81–86)	38–1 (144–146)	40–3 (35–37)	7–1 (20–22)	1–5 (57–60)	10–3 (39–41)	19–1 (24–26)
Core interval: (approx. minimum)	5–5 to 7–1	7–1 to 23–1	25–1 to 37–1	29–1 to 40–1	40–1 to 40–3	7–1 to 21–1	1–5 to 3–4	4–1 to 16–1	16–2 to 19–1
SiO_2	49.29	51.13	50.67	51.16	49.69	50.89	48.09	51.20	48.13
Al_2O_3	21.12	15.00	14.88	16.83	16.88	15.15	22.94	16.53	14.41
Fe_2O_3	2.29	3.27	3.10	2.92	1.65	3.39	1.44	1.80	2.91
FeO	3.52	6.55	7.42	5.44	4.98	6.51	3.27	6.42	6.40
MgO	6.46	7.75	7.74	7.21	10.16	7.49	6.52	7.72	13.75
CaO	14.84	12.60	12.19	12.94	14.21	12.72	15.67	12.75	11.24
Na_2O	1.73	2.11	2.17	2.01	1.58	2.22	1.52	2.10	2.02
K_2O	0.13	0.25	0.27	0.20	0.11	0.29	0.08	0.17	0.16
TiO_2	0.48	1.06	1.23	1.00	0.56	1.07	0.36	1.05	0.76
P_2O_5	0.05	0.16	0.16	0.13	0.07	0.12	0.02	0.11	0.07
MnO	0.09	0.13	0.17	0.15	0.12	0.16	0.09	0.14	0.16
Total	100.00	100.01	100.00	99.99	100.01	100.01	100.00	99.99	100.01
Equiv. glass group	–	332A-b	332A-c	–	–	–	–	332B-a	332B-b
$Mg/(Mg+Fe^{+2})$	0.738	0.639	0.621	0.665	0.791	0.628	0.793	0.689	0.770
NORM. *An/Di*	2.59[a]	1.23	1.25	1.66[a]	1.54	1.17	2.03[a]	1.58[a]	1.46
Ba	25	102	79	73	33	70	23	73	43
Cr	189	90	162	157	411	151	260	199	771
Cu	75	72	69	71	75	72	78	70	89
Ni	83	70	89	80	145	79	103	78	312
Rb	0.9	4.4	4.2	2.8	1.2	3.6	2.3	2.5	2.6
Sr	104	125	114	114	99	106	119	117	89
Y	10.2	23.2	26.3	21.0	11.6	24.7	11.0	23.0	19.2
Zr	35	75	80	68	42	70	32	69	46
Cr/(Cr+Ni)	0.695	0.563	0.645	0.662	0.739	0.657	0.716	0.718	0.712
P/Y	21	28	26	27	26	21	8	21	16
Zr/Y	3.43	3.23	3.04	3.24	3.62	2.83	2.91	3.00	2.40
K/Rb	1199	472	534	593	761	669	289	564	511

Table 2 (continued)

Magma group:	332B-4	332B-5	332B-6a	332B-6b	332B-7a	332B-7b	333A-1	333A-2	333A-3
DSDP sample No. (core section cm interval)	20–1 (91–95)	24–1 (70–72)	21–1 (5–8)	36–6 (58–60)	33–2 (66–69)	48–1 (118–120)	2–2 (36–38)	3–2 (30–31)	6–1 (70–75)
Core interval: (approx. minimum)	20–1 to 20–2	22–1 to 25–1	21–1 to 42–2	36–2 to 37–2	27–2 to 33–2	34–1 to 48–1	1–3 to 2–2	3–1 to 10–1	5–1 to 6–2 (?)
SiO_2	48.61	49.13	47.08	48.96	48.69	50.49	50.93	51.17	50.79
Al_2O_3	14.36	16.63	13.29	18.76	15.24	15.36	14.83	16.95	15.28
Fe_2O_3	2.26	1.99	1.60	2.03	4.22	2.37	2.15	1.85	2.46
FeO	6.67	6.98	6.98	4.53	5.97	5.80	5.83	6.30	6.02
MgO	14.10	10.11	18.64	8.23	7.36	9.79	10.32	7.37	8.92
CaO	11.10	11.74	9.93	14.93	14.69	12.62	12.68	13.05	13.19
Na_2O	1.89	2.32	1.68	1.76	2.21	2.12	1.90	2.16	1.96
K_2O	0.12	0.08	0.09	0.09	0.28	0.17	0.20	0.09	0.17
TiO_2	0.70	0.81	0.52	0.53	1.00	1.00	0.95	0.85	0.95
P_2O_5	0.05	0.06	0.03	0.03	0.12	0.09	0.06	0.06	0.09
MnO	0.15	0.15	0.15	0.14	0.21	0.18	0.16	0.14	0.17
Total	100.01	100.00	99.99	99.99	99.99	99.99	100.01	99.99	100.00
Equiv. glass group	332B-c	332B-d	?	332B-e	–	–	–	–	–
$Mg/(Mg+Fe^{+2})$	0.784	0.723	0.836	0.755	0.614	0.737	0.753	0.681	0.709
NORM. *An/Di*	1.56	1.86[a]	1.74	1.74[a]	0.91	1.32	1.25	1.60[a]	1.24
Ba	42	42	44	30	75	68	78	63	80
Cr	892	444	1426	432	150	480	690	154	411
Cu	83	80	87	86	20	73	82	87	77
Ni	372	174	560	135	92	138	225	70	109
Rb	1.7	1.3	1.6	0.7	5.1	2.4	2.7	0.3	2.8
Sr	86	85	68	106	145	106	145	99	113
Y	18.3	20.3	14.6	15.4	23.0	20.9	20.9	21.1	20.6
Zr	43	49	32	40	57	69	71	n.d.	65
Cr/(Cr+Ni)	0.706	0.718	0.710	0.762	0.620	0.777	0.754	0.688	0.790
P/Y	12	13	9	9	22	19	13	13	20
Zr/Y	2.35	2.41	2.19	2.60	2.48	3.30	3.40	–	3.16
K/Rb	586	665	467	1067	456	588	615	2490	504

Table 2 (continued)

Magma group:	333A-4	333A-5	333A-6	333A-7	334–1	334–2	335	332B-1(X)	332A-1(X)
DSDP sample No. (core section cm interval)	8–1 (72–74)	8–3 (100–103)	9–4 (112–113)	11–1 (91 92)	16–3 (29–31)	20–2 (23–25)	14–4 (130 143)	calculated non-cumulate host liquids	
Core interval: (approx. minimum)	7–1 to 9–5	8–3 to 9–4	9–4 to ?	10–1 to 11–2	16–3 to ?	17–3 to 20–2	5–2 to 16–2		
SiO_2	50.44	49.72	51.21	51.07	51.67	51.69	49.91	49.5	50.1
Al_2O_3	15.13	15.95	16.34	15.74	15.80	15.11	15.57	17.1	16.5
Fe_2O_3	3.20	2.69	2.43	1.85	1.29	1.21	2.03	–	–
FeO	6.67	5.16	5.49	7.21	7.53	6.99	7.41	7.15	8.0[a]
MgO	8.22	8.69	8.80	8.13	8.05	9.13	9.52	10.0	9.5
CaO	12.08	14.90	12.31	12.40	12.29	12.96	11.74	14.0	13.3
Na_2O	2.32	1.78	2.07	2.09	2.04	1.85	2.30	1.54	1.76
K_2O	0.25	0.17	0.13	0.07	0.21	0.06	0.18	0.05	0.14
TiO_2	1.41	0.72	1.01	1.15	0.89	0.78	1.05	0.49	0.50
P_2O_5	0.16	0.06	0.09	0.10	0.08	0.06	0.13	0.07	0.07
MnO	0.12	0.17	0.13	0.18	0.16	0.16	0.15	0.13	0.13
Total	100.00	100.01	100.01	99.99	100.01	100.00	99.99	100.03	100.00
Equiv. glass group	–	–	–	–	–	334	335	–	–
$Mg/(Mg+Fe^{1,2})$	0.651	0.722	0.723	0.674	0.681	0.726	0.698	0.754	0.717
NORM. *An/Di*	1.29	1.13	1.69	1.50	1.52	1.31	1.52	1.7	1.5
Ba	98	59	90	81	84	59	66		
Cr	244	499	130	259	249	155	219		
Cu	40	40	105	70	64	89	68		
Ni	81	120	83	93	114	97	137		
Rb	3.7	1.7	2.6	3.5	2.7	2.1	2.1		
Sr	121	114	133	112	87	76	79		
Y	28.4	17.6	21.2	25.6	22.7	19.8	26.5		
Zr	90	49	65	71	49	41	49		
Cr/(Cr+Ni)	0.751	0.806	0.610	0.736	0.686	0.615	0.615		
P/Y	25	15	19	18	16	14	21		
Zr/Y	3.17	2.78	3.07	2.77	2.16	2.07	1.85		
K/Rb	561	830	415	166	646	237	712		

Table 2 (continued)

Specimen No.		Texture	Phenocrysts	Remarks
332A:	7–1 (66–68)	very coarsely phyric	*pl* ≫ (ol)	cumulate
	23–1 (26–27)	aphyric	(pl + cpx)	cotectic liq.
	26–1 (81–86)	sparsely phyric	pl > cpx > ol	cotectic liq.
	38–1 (144–146)	coarsely phyric	*pl* ≫ cpx	cumulate
	40–3 (35–37)	very coarsely phyric	*pl* + *cpx* > *ol* + (*sp*)	cumulate
	7–1 (20–22)	moderately phyric	pl > cpx ≫ ol	cotectic liq.
332B:	1–5 (57–60)	very coarsely phyric	*pl* ≫ (ol)	cumulate
	10–3 (39–41)	coarsely phyric	*pl* ≫ (cpx > ol)	cumulate?
	19–1 (24–26)	coarsely phyric	*ol* ≫ (*sp* + pl)	cumulate
	20–1 (91–95)	very coarsely phyric	*ol* ≫ (*sp* + pl)	cumulate
	24–1 (70–72)	sparsely-phyric	pl + ol ≫ (cpx)	(glomerophyric; cotectic liq.)
	21–1 (5–8)	very coarsely phyric	*ol* ≫ (*sp*)	cumulate
	36–6 (58–60)	very coarsely phyric	*pl* > *ol* ≫ (*sp*)(?)	cumulate
	33–2 (66–69)	sparsely phyric	ol > pl ≫ sp	cotectic liq.
	48–1 (118–120)	aphyric	(pl)	cotectic liq.
333A:	2–2 (36–38)	sparsely phyric	ol	? cumulate?
	3–2 (30–31)	aphyric	–	cotectic liq.?
	6–1 (70–75)	aphyric	–	cotectic liq.?
	8–1 (72–74)	moderately phyric	pl ≫ cpx + ol	cotectic liq.
	8–3 (100–103)	moderately phyric	*pl* ≧ *cpx* > *ol*(?)	cumulate?
	9–4 (112–113)	sparsely phyric	pl ≫ cpx	cotectic liq.?
	11–1 (91–92)	sparsely phyric	pl > cpx > ol	cotectic liq.
334:	16–3 (29–31)	sparsely phyric	pl > cpx > ol	cotectic liq.?
	20–2 (23–24)	aphyric	(pl)	cotectic liq.
335:	14–4 (130–143)		pl > ol ≫ (cpx)	cotectic liq.

nb. = cumulate phases in italics; microphenocrysts in brackets

The single phase cumulate trends (a) and (b) are clearly related to their respective controlling phase compositions, while 3-phase groups (d) are characterized by strong enrichment trends of P, Ti, Na and Fe. The 2-phase cotectic group (c) shows less intense enrichment of Ti, P and Na, and a slight depletion of Fe. Parental magmas postulated for these low pressure trends may be categorized as high *An/Di* (> 1.4) and low *An/Di* (< 1.4) types, as shown by non-plagioclase-cumulate compositions in Table 2. Low *An/Di* groups have high Ca/Al ratios and high contents of Ti, P and other large ion lithophile (LIL) elements, and are represented by those groups (B-2, A-2, A-3) where coprecipitation of liquidus clinopyroxene with olivine and plagioclase occurs for relatively high contents of MgO. High *An/Di* magmas have low Ca-Al ratios and low contents of LIL elements, and precipitate olivine + plagioclase (B-5) and possibly plagioclase alone (B-1; A-1) on the liquidus. The liquidus crystallization relationships are thus crucial in establishing the divergent derivative chemical trends.

Plagioclase accumulation, commonly evident in Leg 37 lavas (as in many abyssal tholeiites) is not restricted to the high *An/Di* magma groups, but has also affected the low *An/Di* trends of groups such as A-4, B-2, and B-7b (see

Table 3. Phenocryst and groundmass compositional range in magma groups

a) Olivine

Hole no.	Magma Group	Core Interval		wt.% MnO	wt.% Cr_2O_3	wt.% NiO	mole % Fo
332A	332A-1	*7–1*, 66–68	mp	0.15–0.20	0.00–0.05	0.16–0.22	88.3–88.8
332A	332A-2	*21–1*, 101–103	mp	0.20–0.21	0	0.11–0.12	84.6–85.0
332A	332A-1	*28–2*, 109–111	mp	0.21–0.25	0	0.13–0.16	81.7–84.4
332A	332A-4	*29–1*, 65–66	p	0.21–0.21	0	0.15–0.16	84.3–84.5
332A	332A-4	*30–1*, 59–61	p	0.21–0.25	0.04–0.06	0.14–0.15	84.3–84.5
332A	332A-4	*32–1*, 140–142	g	0.21–0.22	0–0.04	0.16–0.20	84.0–84.5
332A	332A-4	*34–2*, 36–38	p	0.21–0.23	0.03–0.05	0.14–0.17	84.2–84.8
332A	332A-4	*36–1*, 21–23	p	0.21–0.24	0.03–0.04	0.13–0.15	84.0–84.4
332A	332A-4	*38–1*, 144–146	g	0.24–0.26	0.04–0.05	0.11–0.13	83.9–84.8
332A	332A-5	*40–1*, 122–124	p	0.16–0.19	0–0.04	0.14–0.22	86.8–89.0
332B	332B-1	*2–5*, 123–125	mp	0.16–0.18	0.05–0.06	0.15–0.20	88.6–89.2
332B	332B-1	*2–6*, 94–97	mp	0.13–0.16	0.03–0.06	0.18–0.21	89.0–89.3
332B	332B-6	*42–2*, 138–140	p	0.13–0.16	0.05–0.08	0.23–0.29	87.9–89.2
333A	333A-2	*3–2*, 30–31	p	0.20–0.25	0.0	0.10–0.18	83.4–86.3
333A	333A-2	*7–4*, 59–61	mp	0.22	0.0	0.11	83.1
335	335-1	*14–4*, 130–143	p	0.14–0.17	0.05–0.05	0.21–0.22	88.4–89.1

b) Cr-Spinel

Hole no.	Magma Group	Core Interval		$100 \cdot Mg/(Mg+Fe^{2+})$	$100 \cdot Cr/(Cr+Al)$
332B	332B-4	*22–1*, 57–60	mp(c)	71.0–67.8	54.8–57.3
332B	332B-4	*22–1*, 57–60	mp(r)	68.7–66.3	51.0–57.3
332B	332B-4	*22–1*, 57–60	incl	73.8–71.6	55.1–55.6

mp = microphenocryst; core (*c*), rim (*r*),
incl = inclusion (in olivine)

below). However, accumulation in these groups is not as extensive as in those groups (B-1, A-1, B-6b) appearing to emanate from high *An/Di* parents. The latter are characterized by distinctly higher values of $Mg/(Mg+Fe^{2+})$ and lower LIL element contents (see Table 2 and Fig. 1), and the composition of accumulating feldspar is slightly more *An*-rich (see Table 3). Parent liquid compositions for B-1 and A-1 magmas have been calculated assuming accumulation of all modal feldspar phenocrysts (an assumption discussed later), and these are given in Table 2. Note the similarity of these compositions to the mafic B-5 lava (e.g. in terms of *An/Di*, Al_2O_3, $Mg/(Mg+Fe^{2+})$, low TiO_2 and P_2O_5), although the latter has higher Na_2O.

The picrite trends B-3, B-4 and B-6a appear to result from olivine accumulation. The analyzed samples are from lithologic sub-units where posteruption

Table 3 (continued)

c) Clinopyroxene

Hole no.	Magma Group	Core Interval		En%	Fs%	Wo%	$100 \cdot Mg/(Mg+Fe^{+2})$
332A	332A-2	*8–1*, 50–52	p	49.5–51.5	8.0–8.7	39.8–42.3	85.5–86.3
332A	332A-2	*14–1*, 101–103	mp	49.7–50.3	7.6–7.9	41.9–42.7	86.3–86.8
332A	332A-2	*21–1*, 31–33	mp	49.9–50.7	6.8–6.9	42.5–43.4	88.1
332A	332A-2	*21–1*, 31–33	gr	52.8–55.1	9.2–12.4	32.5–38.0	81.7–85.1
332A	332A-2	*23–1*, 130–132	mp	49.8–50.6	8.0–9.2	40.2–41.8	84.5–86.3
332A	332A-3	*28–2*, 109–111	mp	49.0–52.8	9.1–10.8	37.6–41.9	82.5–84.7
332A	332A-3	*28–3*, 54–56	gr	49.9–50.2	11.1–13.0	37.0–38.7	79.3–81.9
332A	332A-4	*29–1*, 65–66	gr	46.7–48.5	10.9–11.5	40.0–42.4	80.9–81.1
332A	332A-4	*30–1*, 59–61	gr	47.4–48.8	9.9–10.3	41.4–42.3	82.2–83.2
332A	332A-4	*31–3*, 103–105	gr	42.9–50.2	9.5–23.4	33.7–40.7	64.7–84.0
332A	332A-5	*40–1*, 122–124	p	49.6–51.1	6.0–6.9	42.2–44.1	87.8–89.5
332B	332B-1	*2–5*, 123–125	gr	42.9–45.9	14.5–20.0	36.5–39.6	68.3–76.0
332B	332B-1	*2–6*, 94–97	gr	48.5–50.8	7.8–8.1	41.4–43.4	85.7–86.7
332B	332B-2	*8–3*, 74–76	gr	46.0–54.9	9.4–13.2	34.2–43.8	78.0–83.5
332B	332B-2	*9–2*, 106–108	gr	43.3–46.7	12.3–17.6	39.1–41.1	71.1–79.2
332B	332B-2	*15–1*, 103–105	gr	46.3–53.0	10.0–12.0	36.9–41.8	79.5–83.9
332B	332B-6	*42–2*, 138–140	gr	41.8	13.1	45.1	76.1
333A	333A-2	*3–2*, 30–31	mp	48.1–50.4	7.8–9.8	39.9–42.2	83.7–86.5
333A	333A-7	*11–1*, 91–92	p	48.9–50.8	9.0–10.6	40.2–40.5	82.2–84.9
333A	333A-5	*8–3*, 100–103	p	50.6–51.4	4.9–5.3	43.2–44.5	90.5–91.1
333A	333A-5	*8–3*, 100–103	gr	50.9–52.3	8.3–8.4	39.2–40.8	86.0–86.1
335	335-1	*14–4*, 130–143	gr	40.9	20.8	39.3	66.3

En = enstatite; *Fs* = ferrosilite; *Wo* = wollastonite; mole per cent

olivine settling is clearly evident. The distinction between cumulate and non-cumulate mafic compositions is discussed below in more detail with reference to the solid-liquid partitioning of Fe and Mg. The 3-phase phyric basalt characterizing group A-5 has a bulk chemistry similar to the calculated parent of B-1 group (see Table 2, and Fig. 1). On these grounds it might be interpreted as having crystallized under quasi-equilibrium conditions from the same parent, precipitating clinopyroxene phenocrysts (i.e. with relative suppression of plagioclase) due to higher levels of P_{H_2O} compared to that in B-1 magma (Yoder, 1968; Kushiro and Thompson, 1972), although for reasons discussed below we favor a cumulate hypothesis.

Much of the interlayered sequence of picrite and coarsely plagioclase-phyric lava in the lower part of Hole 332B was initially assigned to one chemical group ('B-6'), assuming the two types to be single-phase cumulate fractions deriving from the same parent magma (Flower et al., 1977). Unfortunately much of this part of the section (about 80 m thick) has been substantially

Table 3 (continued)

d) Plagioclase

Hole no.	Magma Group	Core Interval		Ab%	An%	Or%	M%
332A	332A-1	*7–1*, 66–68	p	8.1–13.6	83.3–89.4	–	2.5–3.1
			g	19.0–20.0	75.4–75.8	0.06–0.11	4.5–5.1
332A	332A-2	*8–1*, 50–52	p	15.7–16.5	80.4–81.4	0.06	2.9–3.1
			g	25.6–26.3	67.3–69.6	0.20–0.40	4.5–6.2
332A	332A-4	*29–1*, 65–66	p	10.3–15.1	81.9–87.4	0.0–0.6	2.1–2.9
			g	33.9	62.2	0.3	3.6
332A	332A-4	*30–1*, 59–60	p	11.7–16.1	80.9–85.7	0.0–0.12	2.6–2.9
332A	332A-4	*31–3*, 103–105	p	10.4–17.7	79.2–87.4	0.0–0.11	2.2–3.0
			g	28.4	66.5	0.3	4.8
332A	332A-4	*32–1*, 140–142	p	11.1–15.5	81.4–85.9	0.0–0.06	2.5–3.1
			g	27.1	62.8	1.6	8.5
332A	332A-4	*34–2*, 36–38	mp	12.2–31.5	64.4–85.3	0.0–0.23	2.5–3.8
			g	27.5	66.8	0.8	5.6
332A	332A-4	*36–1*, 21–23	p	11.3–14.5	82.4–85.7	0.0–0.06	2.6–3.1
332A	332A-4	*38–1*, 144–146	p	10.8–13.1	83.7–86.6	0.0–0.06	2.6–3.1
			g	25.9	69.1	0.2	4.9
332A	332A-5	*40–1*, 122–124	p	11.1–12.2	84.8–86.1	0.0	2.6–3.0
			g	14.1	82.3	0.06	3.6
332B	332B-1	*2–5*, 123–125	p	8.3–10.9	86.6–89.3	0.0	2.2–2.5
			g	26.0	68.2	0.11	5.8
332B	332B-1	*2–6*, 94–97	p	10.1–10.8	86.6–87.3	0.0	2.6
			g	19.6–32.6	61.3–75.6	0.11–0.36	4.7–5.9
332B	332B-2	*8–3*, 74–76	p	10.4–29.4	65.6–87.1	0.06–0.30	2.4–4.7
			g	27.2	68.1	0.2	4.5
332B	332B-2	*9–2*, 106–108	p	9.3–14.7	82.2–88.3	0.0–0.06	2.2–3.0
			g	30.7	64.2	0.2	4.9
332B	332B-2	*15–1*, 103–105	p	10.6–15.7	81.0–86.8	0.06–0.11	2.6–3.1
			g	26.8	68.6	0.2	4.4
333A	333A-5	*9–4*, 5–6	p	11.3–15.2	81.8–86.3	0.0–0.06	2.4–3.2
			g	25.0	70.6	0.2	4.2

p = phenocryst; *mp* = microphenocryst; *gr* = groundmass; *Ab* = albite; *An* = anorthite; *Or* = orthoclase; *M* = $Ca(Mg,Fe)Si_3O_8$; mole per cent
Core section nos. in italics; following nos. refer to cm. intervals

altered so that fractionation hypotheses that do not include secondary phase compositions may be misleading. The relationships of compositions assigned to group B-7 (a and b) are also obscured by alteration, although the subdivision appears to be supported by variation of Zr, P and Y, and also by variation of the Cr/(Cr+Ni) ratio.

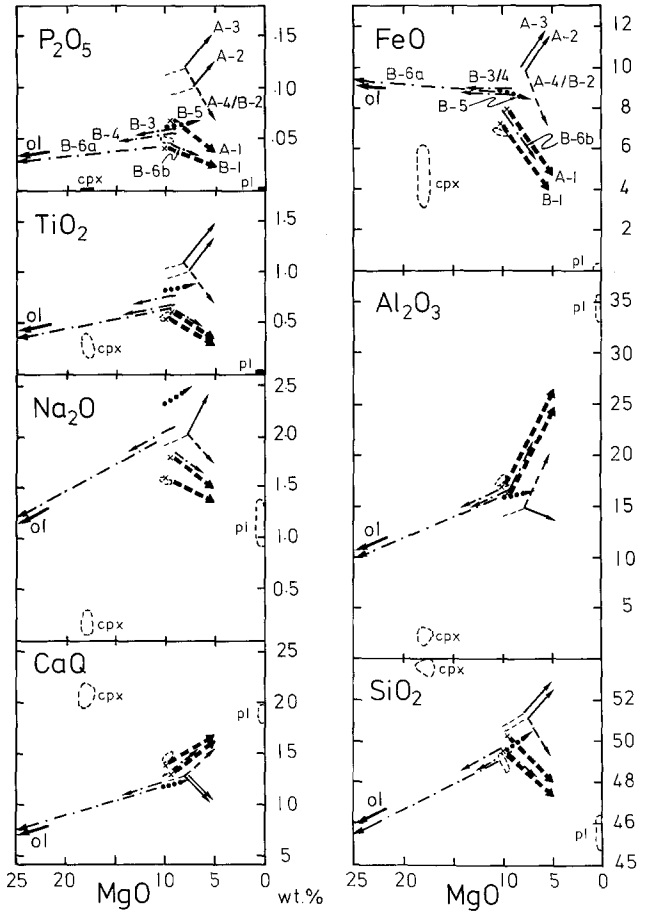

Fig. 1. Schematic diagram of oxide versus MgO variation of magma groups identified at Site 332 (see Flower et al., 1977). 'B'-groups refer to Hole 332B and 'A'-groups to 332A. Compositions of main phenocryst phases are indicated. Symbols are as follows: solid lines = 3-phase (pl + cpx ± ol) cotectic fractionation; thin dashed lines = plagioclase cumulates associated with low *An/Di* magmas; thick dashed lines = plagioclase cumulates associated with high *An/Di* magmas; dotted line = 2-phase (ol + pl) cotectic fractionation; dot-dash lines = olivine cumulates associated with high *An/Di* magmas

Major Element Fractionation Calculations

In order to study the hypothetical processes outlined above, fractionation calculations were set up as mixing problems involving 'parent' (*P*) and 'daughter' (*D*) compositions postulated to be related to each other by addition and/or subtraction of specified mineral phases. We attempted to study three processes or combinations of processes, by resolving sets of equations using the least squares method of Wright and Doherty (1970): (a) fractional crystallization, in which solutions for phenocryst phases (a, b, e, etc.) are forced to be negative; P − a − b − c . . . = D. (b) crystal accumulation, in which phenocryst solutions

are forced to be positive; $P+a+b+c...=D$. (c) 'high pressure processes', reflecting a combination of fractional crystallization and partial melting effects involving orthopyroxene (not observed as a phenocryst phase), for which solutions are not constrained to positive or negative. Similarly, solutions were not constrained for cases where a combination of (a) and (b) were suspected: $P\pm a\pm b\pm c...=D$.

Whole-rock and related phenocryst data for the oxides of Si, Al, Fe^{+2}, Mg, Ca, Na, Ti, P, Mn and Cr were used. K_2O was not used in fractionation calculations because its enrichment in interstitial and vesicular smectite on a fairly wide scale (Robinson et al., 1977) would contribute to high oxide residuals.

Mineral compositions used in the calculations were not left as unconstrained end-members, such as Fo, Fa, An, Ab, etc. Where data were available (Table 3) the most Mg- and/or Ca-rich phenocryst of the respective species present in the supposed parent magma was used. When not available, mineral compositions were selected in accordance with the probable solid-liquid equilibrium (e.g. of Fe/Mg) and by analogy with observed mineral-bulk rock relationships for other groups.

For testing 'intra-group' (i.e. low pressure fractional crystallization) postulates, we follow Wright (1974) in assuming a solution to be potentially valid only if oxide residual (R) are all $\leqq 0.1\%$, ($\Sigma R^2 \leqq 0.1000$). This constraint is compatible with that imposed by analytical precision and accuracy of the data used, although the effect on whole-rock chemistry of alteration has not been completely allowed for. For this reason, parent or daughter rock compositions were only used where $CO_2 \leqq 0.5$ wt. % and $H_2O^+ \leqq 1.0$ wt. %. For the more complex 'inter-group' relationships (i.e. no valid low pressure solution postulated), and for solutions involving chemical analyses from different laboratories (e.g. rock-glass calculations) we consider a solution to be provisionally acceptable if $\Sigma R^2 \leqq 0.4000$, or if R for TiO_2 and P_2O_5 is $\leqq 0.2\%$. The high residuals in some calculations indicate that the parent and daughter compositions in question are probably related by multiple differentiation events rather than by the simple hypothesis proposed. Finally, a solution is only accepted as valid if it is compatible with other observable (e.g. petrographic) constraints. Selected results of fractionation calculations are given in Table 4.

Intra-Group Solutions

For the low *An/Di* whole-rock groups (A-2, A-3, A-4, B-2, B-7a and B-7b), acceptable fractionation solutions involve removal of olivine + pagioclase + clinopyroxene ± Cr-spinel in variable proportions from magnesian parent liquids (Table 4). The solutions are broadly consistent with the observed crystallization assemblages and the oxide versus MgO trends (Fig. 1). They are also closely comparable to solutions for analogous glass pairs (e.g. A−a→A−b; Table 4). However, clinopyroxene solutions for the A-2 group are mostly in excess of observed modal proportions. The high plagioclase component observed in solutions to B-2 intra-group variation (Table 4) probably reflects a certain amount of cumulate plagioclase in the B-2 parent magma (see Fig. 1).

Table 4. Selected phenocryst-liquid redistribution calculations

Postulated Magma Group				Calculated Fractionation Solution					F_{Total}		ΣR
Parent	mg′	Daughter	mg′	ol.	plag.	cpx.	sp.	opx	−	+	
332A-2	0.64	332A-2	0.58	− 2.33	−10.94	− 7.90	*	*	21.17	−	0.0228
332A-a (gl)	0.62	332A-b (gl)	0.55	− 1.90	− 9.60	− 9.20	*	*	20.70	−	0.0294
332A-3	0.62	332A-3	0.60	− 0.89	− 1.52	− 0.43	*	*	2.84	−	0.0862
332A-3	0.62	332A-c (gl)	0.58	− 0.14	− 1.30	− 3.93	*	*	5.37	−	0.0657
332A-4	0.67	332A-4	0.63	− 0.98	− 4.97	− 3.40	*	*	9.35	−	0.0572
332B-2	0.69	332B-2	0.66	− 0.87	− 2.06	− 0.08	*	*	3.01	−	0.0923
332B-2	0.66	332B-a (gl)	0.61	− 2.15	−12.54	− 0.70	*	*	15.39	−	0.1079
332B-5	0.71	332B-5	0.69	− 5.74	− 4.73	−	−0.05	*	15.47	−	0.0986
332B-5	0.71	332B-d (gl)	0.62	− 9.28	−11.94	− 0.26	−0.15	*	21.63	−	0.1390
332B-e (gl)	0.68	332B-6b	0.76	+ 2.19	+20.40	+ 4.08	*	*	−	26.67	0.0465
332B-7a	0.61	332B-7a	0.57	− 2.18	−14.93	−20.34	*	*	37.45	−	0.1284
332B-7b	0.74	332B-7b	0.67	− 4.67	− 2.99	−11.37	*	*	19.03	−	0.1365
332B-2	0.69	332A-4	0.67	− 1.11	+ 0.61	− 0.14	*	*	1.25	0.61	0.0342
332A-4	0.67	332A-3	0.62	+ 6.62	−13.33	− 3.70	−0.18	−9.66	26.87	6.62	0.0490
332A-2	0.63	332A-5	0.79	+15.49	+51.13	+30.02	*	*	−	96.64	0.1602
332B-4	0.78	332B-3	0.76	− 4.87	− 0.98	− 0.97	*	*	6.82	−	0.0040
332B-1	0.74	332B-1	0.72	− 2.10	+27.19	− 0.34	*	*	2.44	27.19	0.0872
332A-1	0.74	332A-1	0.71	− 3.25	+12.40	− 0.51	*	*	3.76	12.40	0.0938

$mg' = Mg/(Mg+Fe^{+2})$; *gl*=glass; *=not involved in fractionation calculation; *F*=weight fraction of total phases and substracted; ΣR=oxide residuals (sum)

Solutions for other glass group pairs (e.g. B−a→A−d; B−c→B−d; B−b→B−d; B−a→A−a; B−a→A−c; B−e→B−d) are not satisfactory in terms of low-pressure fractionation because either the residuals for TiO_2, P_2O_5 or SiO_2 are too high, or a good solution is only obtainable by *adding* as well as subtracting phases. This is clearly not viable for fresh glass compositions and suggests their development independently from each other at low pressure.

Fractionation in the high *An/Di* B-5 group is confirmed to be dominated by removal of olivine + plagioclase ± Cr-spinel, as also shown by associated glass group B−d (Table 4). The solutions for B-6a−6b pairs (picrite-plagioclase-phyric basalt, respectively) reflect a requirement for accumulation of olivine (+Cr-spinel) in the parent and plagioclase in the daughter, but also indicates the need for addition of substantial clinopyroxene, which is not evident in the mode of the plagioclase-phyric (daughter) sub-group. Moreover a better solution is obtained by inclusion of orthopyroxene − implying that the picrites and plagioclase-phyric rocks postulated to belong to the same fractionation system (B-6) have probably developed independently, or at least can only be related through a high pressure regime. Attempts to relate the picrite sub-group to glass group B−e, associated with the plagioclase-phyric rocks, also require addition of clinopyroxene in the solution, although the relation between B−e glass and the plagioclase-phyric sub-group is simple and involves addition mostly of plagioclase with only a small amount of olivine and clinopyroxene (Table 4). Nonetheless, both 6a and 6b 'sub'-groups belong to the high *An/Di* category and are related to parents with high $Mg/(Mg+Fe^{+2})$ ratios and low LIL element contents.

Inter-Group Solutions

The B-5 magma group is the only one of the high *An/Di* type (cf. B-1, A-1, B-3, B-4, B-6a and b) which has not accumulated either olivine or plagioclase. We therefore attempted to relate magnesian members of low *An/Di* groups A-3, B-2, A-2, B-7a and 7b to a primitive B-5 magma, with a $Mg/(Mg+Fe^{+2})$ ratio of 0.72. Although it is reasonably assumed that none of the proposed daughter compositions reflect crystal accumulation, potential 'low pressure' solutions for deriving these magmas from a B-5 type require *addition* of clinopyroxene, while oxide residuals are unacceptable high. Incorporation of orthopyroxene in the calculations reduced ΣR^2 to more acceptable values, but only on condition that subtraction of olivine and plagioclase is accompanied by addition of clinopyroxene and, in some cases, orthopyroxene.

The low *An/Di* group A-3 and the plagioclase-phyric (reflecting plagioclase accumulation in part) A-4 and B-2 groups are stratigraphically contiguous, interlayered or (in the case of B-2) occur at a similar sub-bottom depth. Solutions relating B-2 and A-4 magmas (Table 4) indicate they are virtually the same, with variation expressed simply by redistribution of small quantities of olivine, plagioclase and clinopyroxene. We originally postulated that A-4 magmas were related to A-3 by addition of plagioclase (Flower et al., 1977). However, all calculations attempting to test this for low pressure assemblages give excessively high residuals. The same is true for the pair B-2 – A-3. Mathematically acceptable solutions are achieved for both problems if orthopyroxene is included although the solution for olivine is in each case positive. This result must also reflect a complicated petrogenetic relationship.

The highly phyric 3-phase group A-5 appears to be unique among Leg 37 basalts (except possibly with respect to the moderately phyric 333A-5 group). Despite its apparent chemical similarity to the B-1 parent (see above) it may be distinguished from the latter by its Zr, P and Y concentrations, and by evidence from Fe-Mg partitioning suggesting it to be of cumulate origin (see below). If this is the case, it would almost certainly be related to a magma characterized by 3-phase cotectic fractionation (i.e. of low *An/Di* type). Fractionation calculations support the cumulate hypothesis for A-5 rocks, a moderately good solution being obtained in relation to an A-2 group parent (Table 4).

The picrite groups B-3 and B-4 lie directly above the B-5 glomerophyric group in Hole 332B, and belong to the same apparently continuous pillow sequence. However solutions relating the picrites to B-5 magmas include significant amounts of clinopyroxene which do not occur modally as cumulate phase in the picrites, thus precluding a low pressure relationship. The distinction between B-3 and B-4, however, appears to be minimal (Table 4), as they clearly lie on an olivine accumulation trend. There is, however, a significant, if marginal, difference (expressed in terms of normative *Di* and LIL element content) between the B-3 and B-4 picrites on the one hand and the B-6a picrite cumulates on the other. All are related to high *An/Di* host magmas.

Further Elemental Constraints

The coherence of LIL elements Y, Sr, Ti, Zr, and P appears to be compatible with the groupings made from major element variation (Fig. 2). Phosphorus

is probably the most 'incompatible' element (Anderson and Greenland, 1969) during fractional crystallization of olivine ± plagioclase ± clinopyroxene ± Cr-spinel from basaltic liquid[2], followed by Zr, Ti and then Y. The solid-liquid distribution coefficient (K_D) for Sr exceeds 1 between plagioclase and liquid.

We see in Figure 2 that with progressive increase of Zr content there is a slight decrease of Y/Zr, an approximately constant Ti/Zr ratio. Plagioclase cumulate groups (B-1, A-1 and part of B-7b) are clearly marked by high values of Sr/Zr. The low Zr contents of cumulate groups B-3, B-4, B-6a, B-6b, B-a and A-1 (high *An/Di* magmas) are not entirely due to the dilution effects of added crystals, and there appears to be a hiatus in Zr content between these magmas (and non-cumulate B-5) and those low *An/Di* magmas with higher Zr (which include plagioclase cumulates of A-4, B-2 and B-7b).

The precise amount of solid removal from liquid to produce the observed variation of these elements can be calculated from the Rayleigh Law assuming conditions of surface equilibrium between crystals and liquid, and if distribution coefficients (K_D) for these conditions are known or can be estimated:

$$\frac{C^1}{C^0} = (1-F)^{(K-1)} \tag{1}$$

where: C^1 = concentration of element in derivative liquid;
C^0 = concentration of element in original parent liquid;
F = weight fraction of solid removed;
K = bulk solid/liquid distribution coefficient;
or, for an element pair 'a' and 'b':

$$\frac{(C_a/C_b)^1}{(C_a/C_b)^0} = (1-F)^{(Ka-Kb)}$$

We have selected the element pair P and Y (both analyzed as trace elements), which probably show the greatest divergence of bulk solid/liquid K_D values for basaltic fractionation of the elements analyzed, particularly in regard to clinopyroxene. Thus, fractionation of the P/Y ratio can be almost exclusively attributed to clinopyroxene. This is because the K_D for Y between clinopyroxene and liquid is significantly higher (cf. erbium; Schnetzler and Philpotts, 1970) than that for P (Anderson and Greenland, 1969). We have used equation (1) to calculate from Zr and P data the extent of total solid removed, and equation (2) to calculate from P/Y the extent of clinopyroxene fractionation for each of the hypothetical 'parent-daughter' trends evaluated in terms of major elements.

In Table 5 ranges of Zr and P content for different magma groups are given, together with the ranges of major element parameters *An/Di* and Mg/(Mg+Fe^{2+}). These represent the extremes of intra-group variation for each parameter. Intra-group solutions of F_{total} (as wt. %) for Zr and P variation compare very closely with each other (except for A-4), although predictably they are higher than equivalent major element solutions derived through MDP

[2] There is no evidence from petrography or chemistry that other phases such as apatite, magnetite or garnet are present in the liquidus fractionation assemblages of Leg 37 basalts

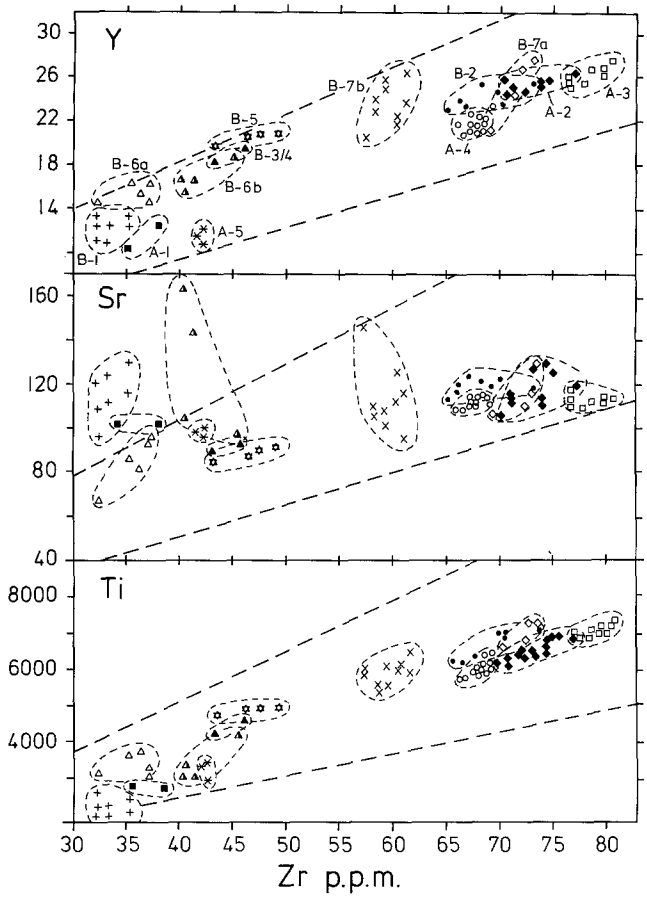

Fig. 2. Plots of Y, Sr and Ti versus Zr (ppm) content for magmas from Site 332 (Holes 332A and 332B). Magma groups identified from major element chemistry are indicated. Lines of equal element/Zr ratio are shown dashed

calculations (cf. Table 4) as they were calculated for extreme compositions of each group. In any case discrepancies arise due to uncertainties of the K_D values and about conditions of crystal-liquid equilibrium during fractionation. In five out of eight intra-group solutions the clinopyroxene component comprises a plausible fraction of F_{total}, within the overall limits of uncertainty, but F_{cpx} values for B-2, -7a and -7b groups are probably somewhat high. With the exception of these results, however, variations of Zr, P and Y are compatible with the interpretations based on major element intra-group variation.

The inter-group calculations show that in terms of Zr, P and Y at least, derivation of low *An/Di* magmas from the high *An/Di* group B-5 would require fractionation of between 50 to 70 wt. % of an almost exclusively clinopyroxene extract. Such a solution is clearly not plausible, either in terms of the observed and predicted phase equilibria (Kushiro, 1973) or the major element mass bal-

Table 5.

Magma Groups	mg′ atomic	*An/Di* normative	Zr range ppm	P range ppm	F^{Zr}_{totals} wt. %	F^{P}_{totals} wt. %	$F^{P/Y}_{cpx}$ wt. %
I Intra-group							
1. 332A-2	0.67–0.58	1.0 –1.25	64–76	510–700	29.2	27.6	14.1
2. 332A-3	0.63–0.59	1.24–1.33	77–81	620–730	9.6	15.3	8.9
3. 332A-4	0.67–0.63	1.23–1.69[a]	66–70	500–650	11.1	23.4	13.1
4. 332B-2	0.69–0.63	0.83–1.70[a]	65–74	390–550	22.8	29.2	20.4
5. 332B-5	0.72–0.70	1.57–1.87	44–49	170–220	23.1	23.2	11.2
6. 332B-6a+b	0.85[b]–0.74	1.55–1.98[a]	32–45	120–200	49.4	40.6	11.2
7. 332B-7a	0.66–0.57	0.91–1.26	70–74	510–560	10.5	9.0	11.2
8. 332B-7b	0.74–0.60	1.18–1.84[a]	54–66	360–540	31.9	33.8	31.8
II Inter-group							
9. 332B-5 332A-3	0.70–0.63	1.57–1.24	43–77	170–620	68.8	73.3	69.7
10. 332B-5 332B-2	0.72–0.69	1.57–0.83	43–65	170–390	56.3	57.1	58.0
11. 332B-5 332A-2	0.72–0.58	1.57–1.00	43–76	170–510	69.4	67.4	64.7

F = calculated % weight fraction of solid (*s*) removed from liquid: using: bulk solid-liquid $K_D^{phosphorus}=0.02$; bulk solid-liquid $K_D^{zirconium}=0.5$; cpx-liquid $K_D^{Yttrium}=0.8$. $mg'=Mg/(Mg+Fe^{+2})$ atomic.

[a] some plagioclase cumulates

[b] some olivine cumulates

ance solutions in Table 4. These relationships may be seen graphically in Figure 3 where intra-group elemental ranges of Zr, P and Y are plotted in a triangular diagram, and in Figure 4 where variation of P/Y ratio with Y content is shown for Site 332 and 333 magmas. It may be assumed that if each magma group represents a separate fractionation system all intra-group elemental variation can be attributed to phenocryst addition or subtraction—almost entirely to clinopyroxene in regard to Zr, P and Y. Each magma group trend is quite distinct in Figure 3. With the exception of Site 334 and 335 magmas (which must belong to totally different mantle melting systems separated in time) the low *An/Di*—derived magma groups (A-2, A-3, A-4, B-2, B-7a and b) plot in a separate region from high *An/Di*-derived groups B-5, B-3, B-4, B-6a and b, and B-1, with *no* perceptible effect imposed by phenocryst accumulation processes. We thus have strong empirical evidence that for any single mantle-melt system Zr, P and Y elemental relationships are highly characteristic of the major high *An/Di* and low *An/Di* categories of primary MORB magma.

Other constraints are provided by 'compatible' (i.e. bulk solid-liquid $K_D > 1$) trace element variation. For instance, variation in terms of $Mg/(Mg+Fe^{+2})$ and $Cr/(Cr+Ni)$ ratios, is a sensitive discriminant between the effects of olivine, clinopyroxene (and also orthopyroxene) and Cr-spinel crystallization, but is not affected by addition or removal of plagioclase (Fig. 5). *Within*-group decrease of $Mg/(Mg+Fe^{2+})$ is accompanied either by an *increase* of $Cr/(Cr+Ni)$ (if olivine is the predominant mafic phase fractionating), or by approximately constant $Cr/(Cr+Ni)$ (if clinopyroxene $\pm$Cr-spinel is coprecipitating). However, the

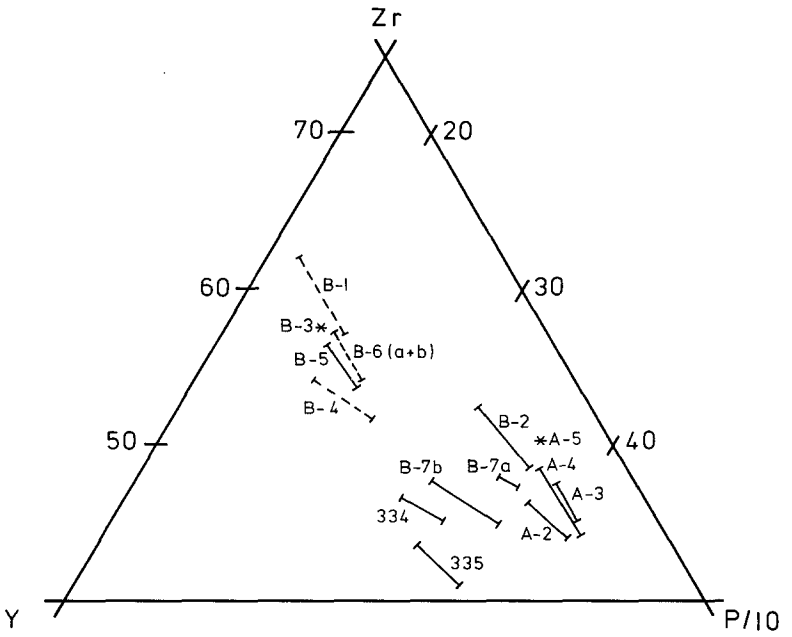

Fig. 3. Calculated intra-group fractionation trends of Zr, P and Y for magma groups from Sites 332 (Holes A and B), 334 and 335. The linear trends represent compositional extremes within each group for which calculated amounts of solid phase removal or addition during fractionation are given in Table 5. Cumulate groups shown by dashed lines. Note the hiatus between high *An/Di* and low *An/Di* magmas from Site 332

overall between-group trend of *decreasing* Cr/(Cr+Ni) with decreasing Mg/(Mg+Fe) appears to reflect clinopyroxene ± Cr-spinel fractionation – although again we must stress this process is not compatible with the major element predictions.

The results of inter-group MDP calculations suggest complex petrogenetic relations – possibly involving several differentiation events. We have already mentioned the possibility of high pressure fractionation of an orthopyroxene-bearing assemblage, resulting in cumulates of the type observed at Site 334. However, no between-group MDP solution was found requiring simple extraction of a 2-pyroxene gabbro or spinel-lherzolite assemblage. Of particular interest is the fact that relations between basic members of high *An/Di* (e.g. B-5) and low *An/Di* magma groups usually require *addition* of clinopyroxene and *removal* of plagioclase (or vice versa), which, if neither phase has been previously fractionated from the respective liquids, must reflect a shift in the plagioclase/clinopyroxene cotectic boundary during partial melting – assuming the magmas to be generated from a plagioclase-bearing peridotite source. A possible influencing factor would be P_{H_2O}. Experimental work by Kushiro and Thompson (1972) on two contrasting primitive abyssal tholeiites shows that variations in P_{H_2O} have a pronounced effect on the phase equilibria of partial melting. Discussion of this and other possible factors is reserved for a separate publication on processes of magma generation beneath MOR spreading axes (Flower and Gibson, in prep.).

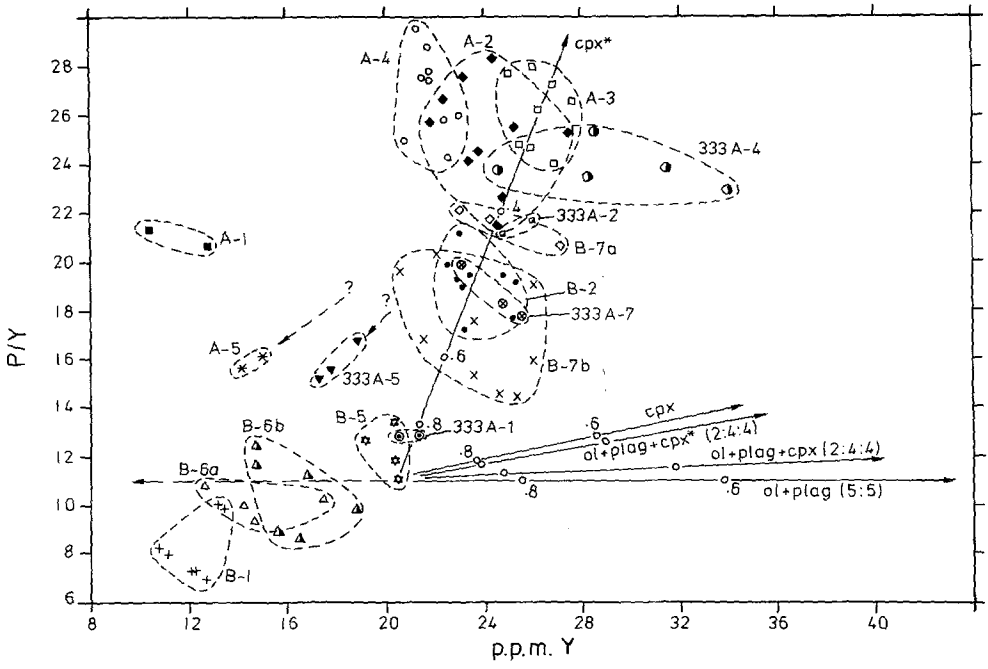

Fig. 4. Plots of P/Y ratio versus Y content for Site 332 and 333 magmas, with major element groupings indicated ('A'- and 'B'-groups refer to respective Holes at Site 332). Calculated trends of variation from a hypothetical B-5 parent are drawn for two alternative cotectic fractionation processes; ol+plag (in a 5:5 ratio) and ol+plag+cpx (in a 2:4:4 ratio) showing the delimiting conditions for extreme values of the K_D for Y between cpx and liquid (0.2 and 0.8). These trends are annotated for weight fraction of liquid remaining during fractional crystallization. Note (a) similarity of high *An/Di* groups 333A-1 (picrite), B-5 (micro-glomerophyric), B-6a (ol-cumulate) and B-1 and B-6b (plag-cumulates), (b) the wide variation of P/Y for low *An/Di* magmas (A-2, A-3, B-2, B-7a and b, etc.), (c) the apparent association of 3-phase cumulate group A-5 and possibly 333A-5 (which has similar petrography) to the low *An/Di* magmas, and (d) the apparently anomalous distinction of A-1 group from the similar B-1 plagioclase-cumulate group (possibly reflecting the inadequacy of interpretations based on 2 major element analyses only).

Cumulate Versus non-Cumulate Magma Compositions

A critical factor in our evaluation of whole-rock compositions is the extent to which they are representative of liquid magmas, evolved or otherwise. The Fe-Mg distribution coefficient K_D, where:

$$K_D = X^{ol}_{FeO} \cdot X^{liq}_{MgO} / X^{liq}_{FeO} \cdot X^{ol}_{MgO}$$

(with X^{ol}_{FeO} = mole fraction of FeO in olivine, etc.) may be used to assess whether olivine phenocrysts are truly in equilibrium with the host rocks in which they occur. The compositions of fresh glass cooling margins are clearly those of

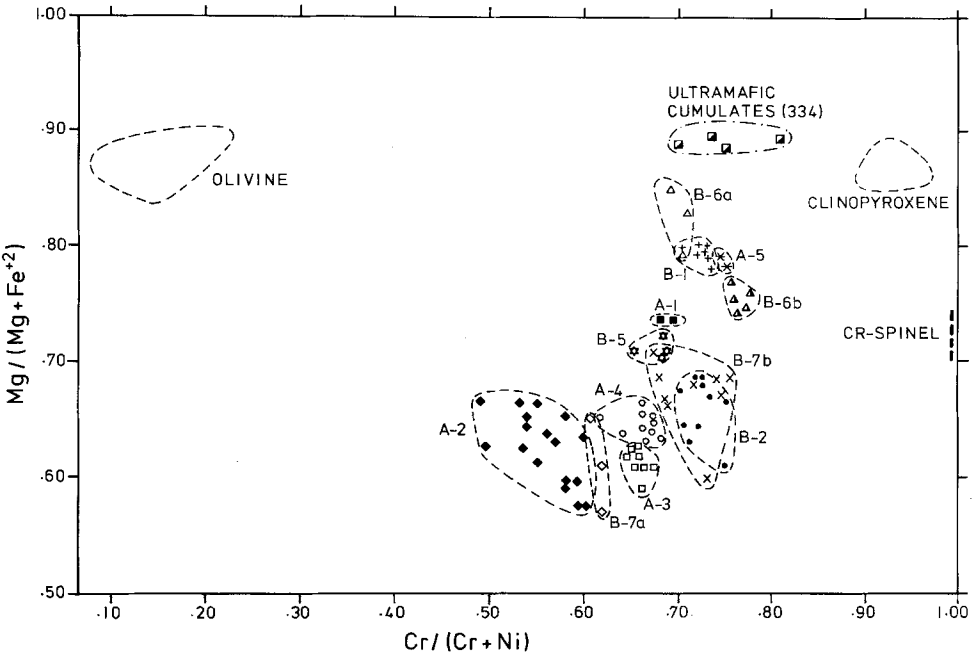

Fig. 5. Plots of $Mg/(Mg+Fe^{+2})$ versus $Cr/(Cr+Ni)$ for Site 332 magmas, showing identity of magma groups, mafic phenocryst phase compositions and Site 334 ultramafic cumulate compositions

liquids, and are valuable for two main reasons: they reflect the lower limit of MgO content and $Mg/(Mg+Fe^{2+})$ ratio in primitive liquids as they do not show the effects of mafic (or other) crystal accumulation; also, the highest K_D for (micro-) phyric olivine in contact with glass may be taken as a minimum true olivine-liquid equilibrium value, while lower K_D values would reflect the case of early-formed olivine phenocrysts coming into contact or close association with *residual* glass, without subsequent equilibration.

Conversely, a value of K_D for olivine/whole-rock (if the whole-rock is postulated to represent a liquid composition and does not comprise a crystal cumulate) should be the same as the maximum olivine/glass K_D value, if the olivine in the glass crystallized from a liquid of the glass composition. A *higher* olivine/whole-rock K_D suggests that the olivine is not in equilibrium, and was introduced from another part of the crystal-liquid system—the most likely mechanism being by crystal settling either within an erupted flow unit during cooling, or prior to eruption in a sub-volcanic magma reservoir. Such K_D values may in any case be compared to those determined experimentally in natural and synthetic systems, or to other empirical observations in natural basaltic liquids.

We have calculated apparent olivine/'liquid' K_D values for associated phenocryst-whole rock and (micro-) phenocryst-glass pairs from among Leg 37 basalts, using data from several workers, the object being to distinguish olivine cumulate compositions from non-cumulates. Calculated K_D values are plotted versus Mg/

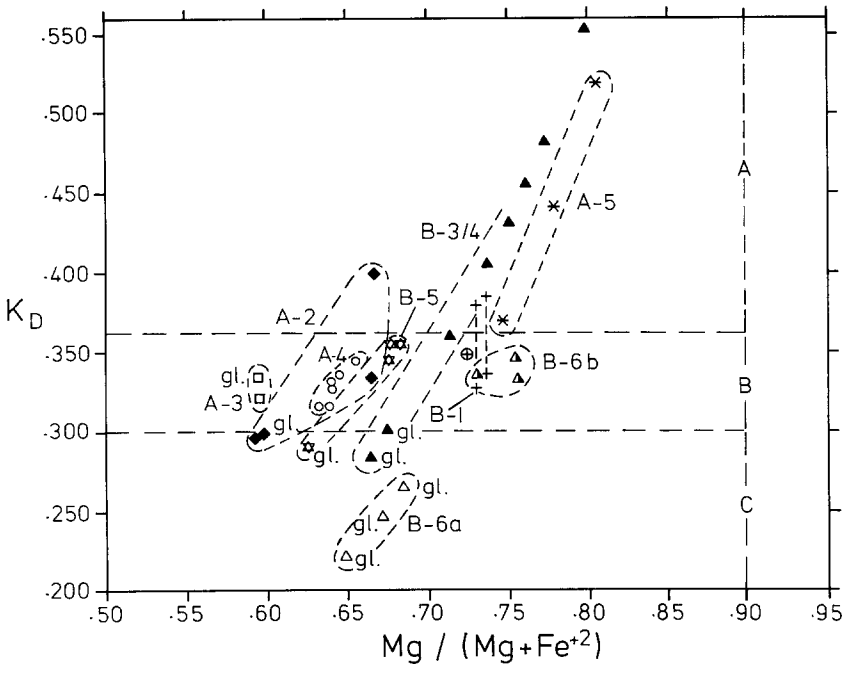

Fig. 6. Plots of the Fe-Mg distribution coefficient between olivine and 'liquid' (K_D)[3] and Mg/$(Mg+Fe^{+2})$ of postulated basaltic compositions. 'Liquid' compositions are those of glass or whole-rock with which respective olivine phenocrysts are associated. From comparison with experimental data and other empirical observations (see text), compositions plotting in fields A, B and C may be interpreted as follows: *A*: olivine (±cpx±pl) cumulates where apparent K_D is too high to be an equilibrium value; *B*: whole-rock or glass compositions which may represent liquids in approximate equilibrium with associated olivine phenocrysts; *C*: glass compositions not in equilibrium with associated olivine phenocrysts, i.e. the latter are locally 'xenocrystic'

$(Mg+Fe^{2+})$ ratio of the whole-rock or glass in Figure 6. The highest K_D calculated for an olivine-glass pair is for two 332A-3 compositions for which $K_D = 0.32$–0.34. This range compares very closely with an average value of 0.33 for a wide range of bulk compositions, pressures and temperatures, predicted by Thompson (1975) and Cawthorne et al. (1973), although it differs slightly from the (higher) value determined by Roeder and Emslie (1970). Close to these are also K_D values (in the range 0.31–0.36) for whole-rock-olivine pairs from glomerophyric (high *An/Di*) B-5 magmas, plagioclase-phyric A-4 magmas and the coarsely plagioclase-phyric A-1, B-1 and B-6b magmas (Fig. 6). Experimental determinations (e.g. Cawthorne et al., 1973) suggest K_D values higher than these are indicative of xenocrystic olivine. Thus, with one exception (Fig. 6), the picrites (B-3; B-4) appear to be cumulates, with olivine phenocrysts too low in Fo to be in equilibrium with a liquid of whole-rock composition, and too high

[3] $K_D = X^{ol}_{FeO} \cdot X^{liq}_{MgO} / X^{liq}_{FeO} \cdot X^{ol}_{MgO}$ (with X^{ol}_{FeO} = mole fraction of FeO in olivine, etc.). For liquid compositions FeO was recalculated assuming $Fe_2O_3 = 1.5$ wt.%, except for 332B-1 magmas (1.0) where the range between values for FeO = total Fe-oxide and measured FeO are indicated. Data for olivine and glass for magma groups B-2 and B-5 were taken from Hekinian et al., 1976

in Fo to have equilibrated with associated residual glass (Fig. 6). Likewise olivine-whole-rock K_D values for the coarsely 3-phase-phyric A-5 rocks are generally too high for these rocks not to be cumulates.

The plagioclase-phyric magmas B-1, A-1 and B-6b have very high ratios of $Mg/(Mg+Fe^{+2})$, ranging from 0.72 to 0.76, some of the highest known for 'abyssal' tholeiite. They appear nonetheless to be in equilibrium with their olivine microphenocrysts (Fo_{89-91}) so their high $Mg/(Mg+Fe^{+2})$ ratio almost certainly reflects a primitive magma composition. The most magnesian of these rocks has an MgO content of 8.7 wt. %, and it is still an open question as to how much plagioclase in this sample *is* cumulate. We see from Figure 6 that at least one 'picrite' (in both the petrographic and chemical senses) is a possible liquid composition. Studies of REE abundance in the plagioclase cumulates and their separated phenocrysts should provide a quantitative answer to this problem (Flower and Gibson, in prep.).

Discussion

The chemical fractionation processes involved in crustal formation at Sites 332 and 333 relate specifically to the 'FAMOUS' region of the MAR (34°–36°N), whose geology and morphology have been studied in detail by French and American scientists (see Moore et al., 1974; Ballard et al., 1975; Bellaiche et al., 1974). Crustal structure in the region has also been well investigated. Whitmarsh (unpubl.) obtained a reversed refraction line over Sites 332 and 333 and found a relatively low velocity upper basement layer (2a). A low velocity upper layer may also exist under the median valley to the east (Whitmarsh, 1973; Poehls, 1974; Fowler and Matthews, 1974). Reconstruction of seismic velocities from drilled material at Leg 37 sites (Hyndman et al., 1976) suggests that the low velocity (less than 4.0 Km/s) layer '2a' consists of fractured volcanic material with intercalated sediment, whereas layer '2b' (4.5–5.5 Km/s) comprises a higher proportion of 'solid' basalt. In Hole 332B the layer 2a/2b transition may be located at about 300 m beneath the sediment-basement interface. The time span envisaged for production of the layer 2 section penetrated in Hole 332B is between 100,000 and 200,000 years, assuming confinement of the eruptive zone to a 2–4 Km-wide median valley and a mean half-spreading rate of 1.17 cm/yr.

It is clear that crustal spreading axes do not conform to any stereotype, whether according to their morphology, magma chemistry, heat flux or tectonic regime. Even within the category 'typical MOR', distinction has to be made between rifted and non-rifted, and slow-spreading and fast-spreading axes in any discussion of chemical and physical models. This paper mainly concerns itself with the nature of magmatic accretion in the FAMOUS environment, and possible constraints on the build-up of the observed crustal structure.

It is reasonable to assume that magmatic differentiation within a short time span at a specific location such as FAMOUS, reflects the interplay of three main factors: fractional crystallization, crystal accumulation and differential partial melting of a (presumed) homogeneous source. The chemistry of the drilled rocks from Leg 37 defines the existence of discrete systems of fractiona-

tion, whereby parent magma batches appear to evolve in temporarily closed systems beneath the zone of magmatic injection and eruption. The emerging picture is complex, but clearly reflects a network of storage chambers and active conduits that tap a range of primary melt composition from the upper mantle. It is envisaged that this pattern is constantly evolving in phase with the overall tectonic framework of crustal spreading. The main questions posed are how typical it may be of spreading axes in general and its compatibility with seismic refraction and other observations in the FAMOUS region.

Cann (1974) recently put forward a generalized model (cf. Cann, 1970) to explain the origin of the ocean crustal structure. An important feature of his model is the existence of a continuous linear magma chamber at the base of the crust where asthenosphere impinges on lithosphere as a result of plastic upward flow. The main basis for this assumption is that transformation from asthenosphere to lithosphere is essentially the continuous filling of the crack produced as two lithospheric plates spread apart from one another. Cann envisages that the lower part of the crust is formed directly by continuous lateral solidification of the axial basal magma chamber, and the upper part by intrusion and eruption of those magmas which escape confinement at depth.

Moore et al. (1974), Ballard et al. (1975) and Hekinian et al. (1976) have adopted a similar model to explain the observed zonation of chemistry in erupted lavas exposed within the FAMOUS median rift. By analogy with Kilauea volcano (Wright and Fiske, 1971) they postulate a compositionally zoned magma chamber extending linearly beneath the median vally, and account for magma variation in terms of olivine and plagioclase fractionation. They prefer this model to other possibilities (e.g. variable primary magmas, differentiation in dikes and sills above a central magma chamber, post-eruptional flow differentiation) because it appears to explain the restriction of relatively young flows to the inner median valley.

Because MOR morphology is probably a function of spreading rate and heat flow, Cann (1974) suggested a minimum spreading rate of marginally less than 1 cm/yr to maintain the thermal balance required to preserve a continuous sub-axial chamber. Sleep (1975) calculated an energy conserving solution for heat flow at MOR's and concluded that for spreading rates below about 1 cm/yr lateral heat conduction away from the ridge precludes the existence of a steady state magma chamber. For higher spreading rates he predicts that some form of chamber must exist due to the lack of opportunity for material to cool, and suggests that a chamber filled with crystal-liquid suspension would be more mechanically stable than a wholly molten magma body.

It is difficult to reconcile such a model with Leg 37 results. Basalts recovered from a single hole (332B) span the entire range of types observed in the surface zonation of median valley eruptions in the FAMOUS area. Because lava flows in the median valleys are observed to have generally flowed less than 500 m from their vents (Moore et al., 1974), the superposition of lavas at Site 332 argues against a zoned distribution. Furthermore, chemical and mineralogical data discussed above clearly indicate that the basalts at Site 332 cannot all be related to a single parent by low pressure fractionation. Instead we see evidence for several primary melts, each modified by varying degrees of shallow level crystallization. Hence, we suggest that Leg 37 basalts can be best explained

by derivation from a number of small separate magma chambers, each of which acts as a temporarily closed system of fractionation. Each chamber may tap either uniquely derived primary magma from the mantle or magma that has undergone varying degrees of high pressure fractionation.

We believe therefore, that the development of lithosphere in the FAMOUS region (spreading rate ca. 2.2 cm/yr) by partial melting, intrusion and eruption of magma, may be seen as an incremental process – in contrast to Cann's (1974) generalized model and to that put forward by Moore et al. (1974), Ballard et al. (1975) and Hekinian et al. (1976). The evidence for complex magma fractionation processes and the vertical interlayering of independently evolved magmas, must be seen in the context of the episodic pattern of eruption evidenced by magnetic stratigraphy (Ade-Hall et al., 1975), the existence of small scale cycles of fractionation with time (Flower et al., 1977), the periodic access of primitive (e.g. 332B-1, -5) magmas to the surface, and the comparatively restricted (up to about 30%) amount of fractionation of oceanic island volcanoes evident from variation within individual magma systems.

On the basis of the Leg 37 results we believe that the distinction between fast and slow spreading ridges, respectively, may be between 'large' steady state magma chamber and a plexus of small chambers, each with its own history of fractionation.

The absence of orthopyroxene in most calculated fractionation assemblages and the compatibility of the latter with observed phenocryst parageneses indicates the bulk of magma fractionation to be a high-level process (less than about 3 Kbars) and not to be confused with that producing orthopyroxene-bearing gabbro and peridotite cumulates drilled at Site 334. These cumulates, which bear no relation to the overlying lavas, are clearly generated at deeper levels, and probably represent the consolidation of magma nearer to the zone of melt segregation (cf. cumulates in ophiolite complexes, e.g. Othris; Menzies and Allen, 1974). Two zones of low shear velocities have been recognized; one at about 30–35 km depth (Solomon, 1973; Girardin, 1975; Steinmetz et al., in press; Ruegg, in press) and one at shallower depths, probably reflecting intra-crustal liquid bodies (Francis and Porter, 1973; Whitmarsh, 1975; Orcutt et al., 1975). Seismic layer 3 might, therefore, be viewed as the result of a mosaic-like coalescence of crystalline bodies of both deep and shallow derivation. Evidence that the Site 334 plutonic melange was intruded as a solid body to the floor of the median rift (Melson et al., 1974; DSDP Leg 37 Init. Rept.) and the seismic properties of these rocks (Hyndman et al., 1976) suggest such a model for layer 3 is possible. The existence of a large continuous magma chamber – at least beneath the MAR – is doubtful, as such a phenomenon would almost certainly eradicate the differences in magma chemistry that we can relate to definable fractionation processes.

Summary

Our main interpretations of Leg 37 geochemistry may be outlined as follows:

1. Primary melts at the FAMOUS spreading axis range in composition from high *An/Di* to low *An/Di* types. High *An/Di* magmas possibly form under

slightly hydrous conditions and are characterized by relatively low LIL-element content, high Al and high $Mg/(Mg+Fe^{2+})$. Contents of Zr, P and Y and their inter-element relationships are highly diagnostic of these two basic categories.

2. As primary magmas rise into the sub-rift environment they are processed through a constantly evolving system of conduits and small magma chambers. Partial or complete solidification occurs with distribution of phenocryst phases by settling or floating.

3. Low pressure liquidus phase relations of primary magmas are dependent on the *An/Di* character, which determines whether *ol*, *ol+pl*, or *ol+pl+cpx*, co-precipitate during initial fractionation. Thus as magma batches become isolated, 'primary' chemical characteristics will be preserved in the erupted products. Cumulate lithologies also characterize the nature of their noncumulate parents: olivine and plagioclase cumulates are commonly derived from high *An/Di* magmas.

4. Fractionation of orthopyroxene-bearing assemblages is evident from Site 334 rocks but is not an important mechanism of lava fractionation, which is presumed to occur mostly at <3 Kbars.

5. The abundance and size of fractionating magma bodies, and frequency and location of eruptions along the spreading axis are a function of rift dynamics, and ultimately of heat flux and spreading rate. These latter factors also determine the chemical nature of primary magmas. The FAMOUS axis is slow spreading and sharply rifted. The possibility that the axis has shifted with time, even during the Brunhes epoch, or that spreading rate is asymmetric (Renard, 1976), may indicate that the region is under relatively great torqued stress.

6. The hypothesis of an extensive magma chamber beneath the rift is not compatible with the chemical and lithologic diversity of Leg 37 magmas at Sites 332 and 333.

Acknowledgments. We extend thanks and appreciation to officers and crew of the D.V. *Glomar Challenger*, DSDP technical staff and our scientific colleagues on Leg 37. Deutsche Forschungsgemeinschaft provided financial support for MFJF and WO, and PTR was in receipt of an Alexander von Humboldt Fellowship. We are grateful to R.N. Thompson and I.L. Gibson for reading and criticizing the manuscript. MFJF wishes to thank Dr. G. Borley and Mr. G. Bullen of Imperial College for advice and assistance with X-ray fluorescence analysis, and also thanks to Professor J. Sutton for granting him facilities as a visiting fellow in the Geology Department at Imperial College. PTR and HUS are grateful to Prof. Trommsdorf for permission to use the microprobe at the ETH Zürich and Drs. M. Engi and J. Sommerauer for help.

References

Ade-Hall, J.M., and shipboard party of DSDP Leg 37: Oceanic basement on the mid-Atlantic Ridge from deep drilling and the sources of the linear magnetic anomaly pattern. Nature **255**, 389–390 (1975)

Anderson, A.T., Greenland, L.P.: Phosphorus fractionation diagram as a quantitative indicator of crystallization differentiation of basaltic liquids: Geochim. Cosmochim. Acta **33**, 493–505 (1969)

Aumento, F.: Magmatic evolution on the mid-Atlantic Ridge: Earth Planet. Sci. Lett. **2**, 225–230 (1967)

Ballard, R.D., Bryan, W.B., Heirtzler, J.R., Keller, G., Moore, J.G., Van Andel, Tj.: Manned submersible observations in the FAMOUS area of the mid-Atlantic Ridge. Science **190**, 103–108 (1975)

Bellaiche, G., Cheminee, J.L., Francheteau, J., Hekinian, R., Le Pichon, X., Needham, H.D., Ballard, R.D.: Rift valley's inner floor: first submersible study. Nature **250**, 558–560 (1974)

Bryan, W.B., Thompson, G., Frey, F.A., Dickey, J.S., Roy, S.: Petrology and geochemistry of basement rocks recovered on DSDP Leg 37. DSDP Initial Rept. **37**, 695–703 (1977)

Cann, J.R.: New model for the structure of the ocean crust. Nature **226**, 928–930 (1970)

Cann, J.R.: A model for oceanic crustal structure developed. Geophys. J.Roy. Astron. Soc. **39**, 169–187 (1974)

Cawthorne, R.G., Ford, C.E., Biggar, G.M., Bravo, M.S., Clarke, D.F.: Determination of the liquid composition in experimental samples: discrepancies between microprobe analyses and other methods. Earth Planet. Sci. Lett. **21**, 1–6 (1974)

Flower, M.F.J., Gibson, I.L.: Primary magma genesis beneath the mid-Atlantic ridge at 36° N. (In preparation)

Flower, M.F.J., Robinson, P.T., Schmincke, H.-U., Ohnmacht, W.: Petrology and geochemistry of igneous rocks. DSDP Initial Rept. **37**, 653–679 (1977)

Fowler, C.M.R., Matthews, D.H.: Seismic refraction experiment using ocean bottom seismographs and sonobuoys in the FAMOUS area. Nature **249**, 752 (1974)

Francis, T.J.G., Porter, I.T.: Median valley seismology: the Mid-Atlantic Ridge near 45°. Geophys. J. **34**, 279–311 (1973)

Girardin, N.: Dispersion des ondes de surface au sud de l'Islande; 3e Reunion, p. 166 (abstr.). Montpellier: Ann. Sci. Terre 1975

Gunn, B.M., Roobol, M.F.: Geochemistry of the igneous rocks, DSDP Leg 37. DSDP Initial Rept. **37**, 735–756 (1977)

Hekinian, R., Moore, J.G., Bryan, W.B.: Volcanic rocks and processes of the Mid-Atlantic Ridge rift valley near 36°49′N. Contrib. Mineral. Petrol. **58**, 83–110 (1976)

Hyndman, R.D., and shipboard party of DSDP Leg 37: Seismic structure of the oceanic crust from deep drilling on the mid-Atlantic ridge. Geophys. Res. Lett. **3**, 201–204 (1976)

Kushiro, I.: Origin of some magmas in oceanic and circum-oceanic regions. Tectonophysics **17**, 211–222 (1973)

Kushiro, I., Thompson, R.N.: Origin of some abyssal tholeiites from the mid-Atlantic ridge. Carnegie Inst. Washington Yearbook **71**, 357–362 (1972)

Melson, W.G., Aumento, F., and shipboard party of DSDP Leg 37: Deep Sea Drilling Project Leg 37: the volcanic layer. Geotimes **19**, pt. 12, 16–18 (1974)

Melson, W.G., Vallier, T.L., Wright, T.L., Byerly, G., Nelen, J.: Chemical diversity of abyssal volcanic glass erupted along Pacific, Atlantic and Indian Ocean sea floor spreading centres. J. Geophys. Res. (Woollard Symposium Vol.), in press (1976)

Menzies, M., Allen, C.: Plagioclase lherzolite–residual mantle relationships within two Eastern Mediterranean Ophiolites. Contrib. Mineral. Petrol. **45**, 197–213 (1974)

Moore, J.G., Fleming, H.S., Phillips, J.D.: Preliminary model for extrusion and rifting at the axis of the mid-Atlantic ridge, 36°48′N. Geology **2**, 437–440 (1974)

Ohnmacht, W., Robinson, P.T., Schmincke, H.-U., Flower, M.F.J.: Mineral chemistry of eruptive rocks: DSDP Leg 37. (In preparation)

Orcutt, J., Kennet, B., Dorman, L., Prothero, W.: A low-velocity zone underlying a fast spreading rise crest. Nature **256**, 475–476 (1975)

Poehls, K.: Seismic refraction on the mid-Atlantic ridge at 36°N. J. Geophys. Res. **79**, 3370–3373 (1974)

Renard, V.: Evolution of the mid-Atlantic ridge at the FAMOUS latitude from geophysical data; Proc. of special workshop on ocean crust, Brest, Nov., 1975. Bull. Soc. Geol. Fr. (in press)

Robinson, P.T., Flower, M.F.J., Schmincke, Ohnmacht, W.: Low Temperature alteration of oceanic basalts, DSDP Leg 37. DSDP Initial Rept. **37**, 775–793)1977)

Roeder, P.L., Emslie, R.F.: Olivine-liquid equilibrium. Contrib. Mineral. Petrol. **29**, 275–289 (1970)

Ruegg, J.C.: Main results about the crustal and upper-mantle structure of the Djibouti region (T.F.A.I.). Afar-Monographie (in press)

Schnetzler, C.C., Philpotts, J.A.: Partition coefficients of rare earth elements between igneous matrix material and rock-forming mineral phenocrysts–II. Geochim. Cosmochim. Acta **34**, 331–340 (1970)

Sleep, N.H.: Formation of ocean crust: some thermal constraints. J. Geophys. Res. **80**, 4037–4042 (1975)
Solomon, S.C.: Shear-wave attenuation and melting beneath the mid-Atlantic ridge. J. Geophys. Res. **78**, 6044–6059 (1973)
Steinmetz, L., Hirn, A., Sapin, M., Whitmarsh, R., Moreira, V.: Zones of P-wave attenuation beneath the crest of the mid-Atlantic ridge. (In press)
Thompson, R.N.: Primary basalts and magma genesis, II. Snake River Plain, Idaho. Contrib. Mineral. Petrol. **52**, 213–232 (1975)
Whitmarsh, R.B.: Median valley refraction line, Mid-Atlantic ridge at 37°N. Nature **246**, 297–299 (1973)
Whitmarsh, R.B.: Axial intrusion zone beneath the median valley of the mid-Atlantic ridge at 37°N. detected by explosion seismology. Geophys. J. **42**, 189–215 (1975)
Wright, T.L., Presentation and interpretation of chemical data for igneous rocks. Contrib. Mineral. Petrol. **48**, 233–248 (1974)
Wright, T.L., Doherty, P.C.: A linear programming and least squares computer method for solving petrologic mixing problems. Geol. Soc. Am. Bull. **81**, 1995–2008 (1970)
Wright, T.L., Fiske, R.S.: Origin of the differentiated and hybrid lavas of Kilauea volcano, Hawaii. J. Petrol. **12**, 1–65 (1971)
Yoder, H.S.: Experimental studies bearing on the origin of anorthosite. N.Y. State Mus. Sci. Serv. Mem. **18**, 13–22 (1968)

Received January 3, 1977 | Accepted in revised form June 22, 1977